BUTTERWORTH HEINEMANN

Numerical investigation of the sealing capacity of centrifugal instabilities in shaft seals

C. A. Vionnet
Department of Aerospace and Mechanical Engineering, The University of Arizona, Tucson, AZ, USA

The study of a thin, incompressible Newtonian fluid layer trapped between two almost parallel, sliding surfaces has been actively pursued in the last four decades. This subject includes lubrication applications such as slider bearings or the sealing of nonpressurized fluids with shaft seals. In the present work, the flow of lubricant fluid through a microgap formed beween a synthetic seal and a rotary shaft is first analyzed using scaling arguments and then numerically. The study is initially carried out assuming that a "small-gap" parameter δ attains an extreme value in the Navier–Stokes equations. The precise meaning of small gap is achieved by the particular limit $\delta = 0$, which, within the bounds of the hypotheses, predicts transport of lubricant through the sealed area by centrifugal instabilities. The incidence of temperature variations attributable to viscous dissipation of mechanical energy in the fluid properties is also investigated. Numerical results obtained with the finite element method are presented. In particular, the influence of inflow and outflow boundary conditions and their impact in the simulated flow are discussed.

Keywords: lip seals; small gap; Navier-Stokes; centrifugal instabilities; open boundaries; penalty method; finite elements

Introduction

This paper deals with a type of synthetic seal, commonly used in automobiles, that operates under all weather conditions. These elastomeric devices seal slightly pressurized oil trapped inside the ball bearings container keeping the lubricant free of impurities from the outside (Figure 1). The seal, rigidly bonded to the oil reservoir, is stationary and presents a narrow section that slides over the moving surface of the rotary shaft. When the seal is assembled over the shaft, the lip edge is distorted, and a dry contact surface is formed. However, Jagger (1957) found that under approximate steady-state conditions, the contact lip runs over a very thin fluid film that separates the seal from the shaft. Since then, researchers have been trying to explain the generation of the hydrodynamic force able to sustain a gap between the two bodies, and the mechanisms that prevent the fluid from leaking through. Jagger put forward the idea that the surface tension of the sealed fluid controls leakage by means of a meniscus formed on the air side. Years later, Jagger and Walker (1966) proposed that asperities acting as microbearing pads were partially responsible for the hydrodynamic lift. Kawahara and Hirabayashi (1977) observed that a seal leaks when the installation is reversed. Kawahara *et al.* (1980) studied the possible contribution of seal asperities in the sealing mechanisms. Lebeck (1986a,b), however, concluded that the existing models could not fully explain the sliding motion as commonly observed in experiments. A more recent work showed that a properly installed and functional lip seal exhibits a net transfer of lubricant from the low-pressure region to the high-pressure region (Stakenborg 1988). Salant (1992) claimed that microundulations in the lip surface restrict leakage by virtue of a "reverse-pumping" process in which fluid is driven from the low- to the high-pressure side, but no clear experimental evidence supporting these kind of asperities action has yet been reported.

An alternative line of analysis is given by the so-called elastohydrodynamic lubrication theory (EHL). It is known that whenever an incompressible fluid is forced to flow between a compliant body and a rigid one, the subsequent deformation of the elastic body affects the flow field of the viscous lubricant. The solution of the interaction between the fluid film and the compliant body, therefore, must be sought through an iterative procedure. The classical approach is to relate the film thickness to the fluid pressure using Hertzian point contant theory (Oh and Rohde 1977; Taylor and O'Callagham 1972; Verstappen and van Groesen 1989). Variants of the EHL theory have been applied to rectangular, reciprocating elastomeric seals with considerable success (Prati and Strozzi 1984; Ruskell 1980). However, the large number of parameters needed to describe any EHL model for lip seals makes the approach difficult to implement (Vionnet 1993). The existence of roughness comparable in size to the thickness of the fluid layer certainly complicates any mathematical description of the problem (Salant and Flaherty 1995; Serbetci and Tichy 1991). Part of the intricate nature of the problem lies in the disparate length scales representing the geometry of the real system. Nevertheless, by considering a rigid lip seal, it is possible to formulate a one-side model based on a proper interpretation of these scales. It will be established that this approach provides a deeper understanding of the way in which shaft seals work.

Address reprint requests to Prof. C. A. Vionnet, FICH. Universidad Nacional del Litoral, CC 495, 3000 Santa Fe, Argentina.

Received 20 January 1995; accepted 6 May 1995

Int. J. Heat and Fluid Flow 16: 254–262, 1995

655 Avenue of the Americas, New York, NY 10010

0142-727X/95/$10.00
SSDI 0142-727X(95)00029-P

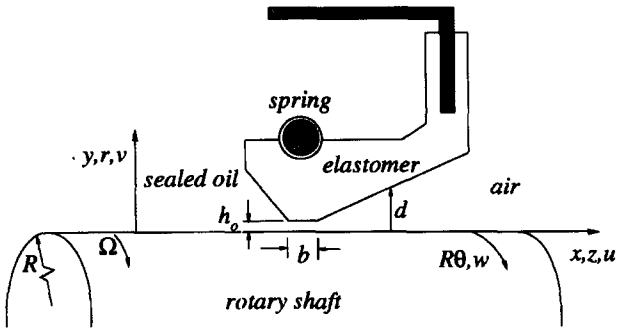

Figure 1 Schematic of lip seal for rotary shaft application

The first stage of this study is carried out assuming that a "small-gap" parameter δ attains an extreme value in the Navier–Stokes equations. The precise meaning of small gap is achieved by the particular limit $\delta = 0$ which, within the bounds of the hypotheses, predicts transport of lubricant through the sealed area by centrifugal instabilities. In the next section, the small-gap equations are obtained using a rather simple order-of-magnitude analysis. The effect of the temperature distribution on the fluid properties and on the velocity field in the contact area is also investigated. Numerical results obtained with the penalty function approximation in the finite element method are presented. In particular, the influence of inflow and outflow boundary conditions, and their impact in the simulated flow are discussed.

Analytical model

The oil–film is considered already formed under normal working conditions. Neither mechanical contact between the sealing surfaces nor elastic distortion of the outer elastic seal is allowed. The thin viscous liquid layer is assumed to be bounded above by a smooth surface and below by a perfectly rounded shaft. Edge effects, such as the meniscus experimentally observed on the air side, are also ignored. Despite the fact that the film within the gap is very thin, it is assumed to be thick enough to conform to the continuum hypothesis of the liquid. There is no local rupture of the film, such as cavitation or dry spots in the contact area, and the layer consists of an incompressible Newtonian fluid with variable properties.

For the present problem, the analysis of the fluid motion involves, roughly speaking, three disparate length scales (Figure 1); namely, the radius R of the shaft [O(0.04 m)], the much smaller thickness h_o of the fluid in the contact area [O(10 μm)], and an intermediate length b characterizing the axial extent of the contact region [O(200 μm)]. Regardless of the flow structure within the gap, the velocity field in the neighboring regions is clearly affected by the different size of the approaching channels. Therefore, for a fluid film of average thickness d and characteristic viscosity v_o, only one velocity scale can be formed in the outer regions; namely, v_o/d. The other scale is clearly the sliding velocity ΩR, where Ω is the angular velocity of the rotary shaft. Denoting the time with t, the dynamic pressure with p^*, the velocity components with (u_z, u_r, u_θ) in the directions (z, r, θ), respectively, and the temperature with T, the flow field equations (see Appendix) are rescaled by writing the following:

$$(x, y) \to \left(\frac{z}{d}, \frac{r-R}{d}\right) \quad , \quad \tau \to \frac{v_o t}{d^2} \quad , \quad p \to \frac{p^* d^2}{\rho v_o^2}$$

$$(u, v, w) \to \left(\frac{d}{v_o}u_z, \frac{d}{v_o}u_r, \frac{u_\theta}{\Omega R}\right) \quad , \quad \phi \to \frac{T - T_\infty}{T_o - T_\infty} \qquad (1)$$

The fluid properties are density ρ, absolute viscosity $\mu^* = \mu^*(T)$, specific heat $c = c(T)$, and thermal conductivity $k = k(T)$, with the understanding that an asterisk denotes dimensional quantities. The characteristic values are some reference temperature T_o, a sink temperature T_∞ deep inside the solid, and a reference viscosity $\mu_o^* = \mu^*(T_o)$ so that $\mu_o^* = \rho v_o$. It can be seen that, in the limit $\delta = d/R \to 0$, the equations of motion reduce to the following:

$$\nabla \cdot \mathbf{u} = 0 \qquad (2)$$

$$(\partial_\tau + \mathbf{u} \cdot \nabla)u = -\partial_x p + \nabla \cdot \mu \nabla u + \partial_x \mathbf{u} \cdot \nabla \mu \qquad (3)$$

$$(\partial_\tau + \mathbf{u} \cdot \nabla)v = -\partial_y p + \nabla \cdot \mu \nabla v + \partial_y \mathbf{u} \cdot \nabla \mu + T_a w^2 \qquad (4)$$

Notation

B_r	Brinkman number, $= P_r E_c$
b	width of the seal lip
c	specific heat of the fluid
d	average fluid thickness outside the contact region
k	thermal conductivity of the fluid
h	convection heat transfer coefficient
h_o	film thickness within the gap
$O(\ )$	Order of magnitude, on the order of
p^*	dimensional fluid pressure
p	dimensionless fluid pressure
R	radius of the shaft
T	fluid temperature
T_o	reference temperature
T_∞	sink temperature
t	dimensional time
(u_z, u_r, u_θ)	dimensional fluid velocity components in the cylindrical coordinates, z, r, θ
(u, v, w)	dimensionless fluid velocity components in the dimensionless coordinates, x, y, θ
W	weight or test function in the method of the weighted residuals
E_c	Eckert number
N_u	Nusselt number, $= hd/k$
P_r	Prandtl number
R_e	Reynolds number, $= \Omega R h_o / v_o$
T_a	Taylor number

Greek

δ	small-gap parameter, $= d/R$
λ	penalty parameter, $= 10^8$
μ^*	dimensional fluid viscosity
μ	dimensionless fluid viscosity
v_o	dimensional kinematic viscosity of the fluid at the reference temperature
ρ	fluid density, constant
σ_{ij}	dimensionless stress tensor for a Newtonian fluid
τ	dimensionless time
ϕ	dimensionless temperature
φ_i	Galerkin basis function with compact support on node i
Ω	angular velocity of the rotary shaft
ω	interior of the computational domain and $\partial\omega$ its boundary
∂_x	partial derivative with respect to x, $= \dfrac{\partial}{\partial x}$

$$(\partial_\tau + \mathbf{u}\cdot\nabla)w = \nabla\cdot\mu\nabla w \tag{5}$$

$$(\partial_\tau + \mathbf{u}\cdot\nabla)\phi = \nabla\cdot\frac{1}{P_r}\nabla\phi + E_c\mu[(\partial_x w)^2 + (\partial_y w)^2] \tag{6}$$

Above, $\mathbf{u}=(u, v)$ is the velocity vector and $\nabla=(\partial_x, \partial_y)$ is the gradient operator, both defined in the axial plane x, y. The relevant parameters here are the Taylor number T_a, the Prandtl number P_r, the Eckert number E_c, and the relative viscosity μ defined as follows:

$$T_a = \frac{\Omega^2 R d^3}{\nu_o^2}, P_r = \frac{\rho c \nu_o}{k}, E_c = \frac{(\Omega R)^2}{c(T_o - T_\infty)}, \mu = \frac{\mu*}{\mu_o^*} \tag{7}$$

The above system of equations is a generalization of the so-called small-gap equations, widely used in the study of the stability of axisymmetric Taylor–Couette flows (Chandrasekhar 1961; Hall 1975). Note that although curvature effects are almost completely neglected, they are retained through the centrifugal term by holding the Taylor number fixed as $\delta \to 0$. It follows that a rigid seal separated from a rotary shaft by a thin lubricating film is subject to centrifugal instabilities on either side of the contact area; instabilities that, in turn, may drive a secondary flow across the gap.

Boundary conditions

The computational domain is depicted in Figure 2. The size of the gap h_o in the contact surface (see Figure 1) is assumed to be equal to 10 μm. The width of the seal lip is set equal to 200 μm and is used as the characteristic length d. The two angles of approach are 60° from the oil side and 12° from the air side. The boundary conditions are the usual: no slip and no mass penetration at solid walls. That is, $u=v=0$, and $w=1$ at the lower boundary $y=0$, which represents the outer surface of the rotating shaft, and $u=v=w=0$ at the upper boundary, which is stationary. The boundary conditions for the temperature are those indicated in Figure 2. At the artificial boundaries, on both sides of the contact region, the free-boundary condition (FBC) proposed by Papanastasiou et al. (1992) is used. Essentially, the FBC retains the contribution of the line integrals along the open boundaries in the discretized equations of the weak form. For comparison purposes, the stress-free or natural boundary condition (NBC) is also employed. Both open boundary conditions (OBC) are exhaustively analyzed in the author's thesis for a variety of situations exploiting the analogy between a homogeneous rotating fluid and a nonrotating, stratified fluid (Chandrasekhar 1961; Veronis 1967). This subject is still an active field of research (Gresho and Sani 1990), but additional details can be found in the works of Sani and Gresho (1994) and Heinrich and Vionnet (1995). The natural boundary condition $\partial_n = 0$ is used in the weak form of Equations 5 and 6.

Finite element formulation

The numerical solution of Equations 2–6 is based on the Galerkin formulation of the method of weighted residuals using the primitive variable form of the Navier–Stokes equations. The weak form of the governing equations is first expressed in Cartesian tensor notation as follows:

$$\int_\omega \left[W_i\left(\frac{\partial u_i}{\partial t} + u_j\frac{\partial u_i}{\partial x_j}\right) + \frac{\partial W_i}{\partial x_j}\sigma_{ij}\right] d\omega = T_a\int_\omega W_i\delta_{i2}w^2 d\omega + \int_{\partial\omega} W_i\sigma_{ij}n_j\, ds \tag{8}$$

$$\int_\omega \left[W\left(\frac{\partial w}{\partial t} + u_j\frac{\partial w}{\partial x_j}\right) + \mu\frac{\partial W}{\partial x_j}\frac{\partial w}{\partial x_j}\right] d\omega = \int_{\partial\omega} W\mu\frac{\partial w}{\partial x_i}n_i ds \tag{9}$$

$$\int_\omega \left[W\left(\frac{\partial \phi}{\partial t} + u_j\frac{\partial \phi}{\partial x_j}\right) + \frac{1}{P_r}\frac{\partial W}{\partial x_j}\frac{\partial \phi}{\partial x_j}\right] d\omega = \int_\omega W\mu E_c\frac{\partial w}{\partial x_j}\frac{\partial w}{\partial x_j}d\omega + \int_{\partial\omega} W\frac{1}{P_r}\frac{\partial \phi}{\partial x_i}n_i\, ds \tag{10}$$

where $\mathbf{n}=n_i$ is the unit normal vector pointing outward from the boundary $\partial\omega$ of the domain ω, $W_i=(W_1, W_2)$ and W are weighting functions, $\mathbf{u}=u_i$ is the velocity vector with u, v components in $\mathbf{x}=x_i$ directions, δ_{ij} is the Kronecker delta, and σ_{ij} is the stress tensor for a Newtonian fluid given by the following:

$$\sigma_{ij} = -p\delta_{ij} + \mu\left(\frac{\partial u_i}{\partial x_j} + \frac{\partial u_j}{\partial x_i}\right) \tag{11}$$

For a partition of the domain into N_e finite elements and N nodes, the dependent variables u, v, and ϕ are now expanded in the standard Galerkin basis functions

$$\{\varphi_i(\mathbf{x})\}_{i=1}^N$$

using bilinear quadrilateral elements. The dynamic pressure is eliminated from the problem, except at the boundaries, by penalizing the incompressibility constraint with the pseudoconstitutive relation (Hughes et al. 1979)

$$p = -\lambda\frac{\partial u_i}{\partial x_i} \tag{12}$$

All terms of the weak form of the governing equations are evaluated with full Gaussian quadrature, except the penalty term where selective reduced integration is employed (Carey and Oden 1986). The weighting functions are set equal to the basis function with the exception of the convective terms, where perturbed

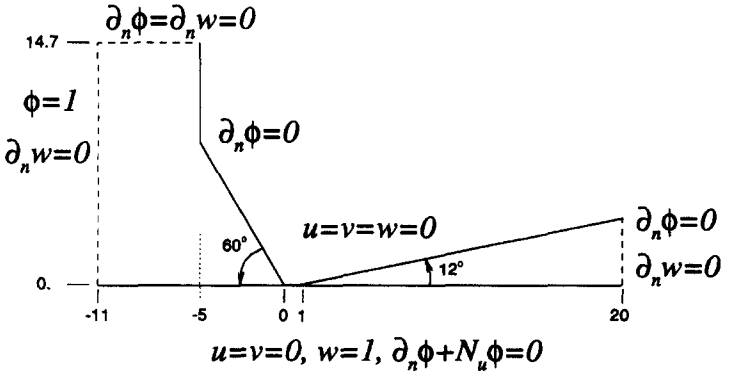

Figure 2 Computational domain and boundary conditions

Petrov–Galerkin functions with balancing tensor diffusivity are employed (Kelly et al. 1980). The centrifugal acceleration term is evaluated using the procedure known as product approximation (Christie et al. 1981). For a single connected domain ω with boundary $\partial\omega = \partial\omega_P + \partial\omega_A$, where $\partial\omega_P$ is the physical part of the boundary $\partial\omega$, and $\partial\omega_A$ is the artificially defined portion of $\partial\omega$, the calculation of the line integral in Equation 8 is carried out using an appropriate set of one-dimensional (1-D) functions. The application of the Galerkin method leads to the following semidiscrete weighted residuals approximation

$$\begin{bmatrix} M & 0 \\ 0 & M \end{bmatrix}\begin{bmatrix} \dot{\underline{\mathbf{u}}} \\ \dot{\underline{\mathbf{v}}} \end{bmatrix} + \begin{bmatrix} \underline{c}\,(\mathbf{u};\underline{u}) \\ \underline{c}\,(\mathbf{u};\underline{v}) \end{bmatrix} + \begin{bmatrix} B_{11} & B_{21}^T \\ B_{21} & B_{22} \end{bmatrix}\begin{bmatrix} \underline{\mathbf{u}} \\ \underline{\mathbf{v}} \end{bmatrix} = \begin{bmatrix} \underline{\mathbf{b}}_{\mathbf{u}} \\ \underline{\mathbf{b}}_{\mathbf{v}} \end{bmatrix} \tag{13}$$

$$\begin{bmatrix} M & 0 \\ 0 & M \end{bmatrix}\begin{bmatrix} \dot{\underline{\mathbf{w}}} \\ \dot{\underline{\phi}} \end{bmatrix} + \begin{bmatrix} D(\mathbf{u}) + A(\mu) & 0 \\ 0 & D(\mathbf{u}) + A(\frac{1}{Pr}) \end{bmatrix}\begin{bmatrix} \underline{\mathbf{w}} \\ \underline{\boldsymbol{\Phi}} \end{bmatrix} = \begin{bmatrix} \underline{\mathbf{b}}_{\mathbf{w}} \\ \underline{\mathbf{b}}_{\phi} \end{bmatrix} \tag{14}$$

Above, $\underline{\mathbf{u}} = (u_1, u_2, \ldots, u_N)$, $\underline{\mathbf{v}} = (v_1, v_2, \ldots, v_N)$, $\underline{\mathbf{w}} = (w_1, w_2, \ldots w_N)$ are the vectors of the unknown nodal velocities, $\underline{\boldsymbol{\Phi}} = (\phi_1, \phi_2, \ldots, \phi_N)$ is the vector of the unknown nodal temperatures, and $\cdot \equiv \mathrm{d}/\mathrm{d}t$. The matrices M, B_{mn} $(m, n = 1, 2)$, D, A, and the vectors $\underline{\mathbf{c}}$, $\underline{\mathbf{b}}_{\mathbf{u}}$, $\underline{\mathbf{b}}_{\mathbf{v}}$, and $\underline{\mathbf{b}}_{\phi}$ are given by the following:

$$m_{ij} = \int_\omega \varphi_i \varphi_j \, \mathrm{d}\omega \tag{15}$$

$$b_{11_{ij}} = \lambda \int_\omega \frac{\partial\varphi_i}{\partial x}\frac{\partial\varphi_j}{\partial x}\mathrm{d}\omega + \int_\omega \mu\left(2\frac{\partial\varphi_i}{\partial x}\frac{\partial\varphi_j}{\partial x} + \frac{\partial\varphi_i}{\partial y}\frac{\varphi_j}{\partial y}\right)\mathrm{d}\omega \tag{16}$$

$$b_{21_{ij}} = \lambda \int_\omega \frac{\partial\varphi_i}{\partial y}\frac{\partial\varphi_j}{\partial x}d\omega + \int_\omega \mu\frac{\partial\varphi_i}{\partial x}\frac{\partial\varphi_j}{\partial y}d\omega \tag{17}$$

$$b_{22_{ij}} = \lambda \int_\omega \frac{\partial\varphi_i}{\partial y}\frac{\partial\varphi_j}{\partial y}\mathrm{d}\omega + \int_\omega \mu\left(\frac{\partial\varphi_i}{\partial x}\frac{\partial\varphi_j}{\partial x} + 2\frac{\partial\varphi_i}{\partial y}\frac{\partial\varphi_j}{\partial y}\right)\mathrm{d}\omega \tag{18}$$

$$a(\mu)_{ij} = \int_\omega \mu\left(\frac{\partial\varphi_i}{\partial x}\frac{\partial\varphi_j}{\partial x} + \frac{\partial\varphi_i}{\partial y}\frac{\partial\varphi_j}{\partial y}\right)\mathrm{d}\omega, \quad i,j = 1,\ldots,N \tag{19}$$

$$c(\mathbf{u},u)_i = \sum_k\sum_j\left(\int_\omega\left(\varphi_i + \frac{\tilde{k}\mathbf{u}\cdot\nabla\varphi_i}{\|\,\mathbf{u}\,\|^2}\right)\left(u_j\varphi_j\frac{\partial\varphi_k}{\partial x} + v_j\varphi_j\frac{\partial\varphi_k}{\partial y}\right)\mathrm{d}\omega\right)u_k \tag{20}$$

$$c(\mathbf{u},v)_i = \sum_k\sum_j\left(\int_\omega\left(\varphi_i + \frac{\tilde{k}\mathbf{u}\cdot\nabla\varphi_i}{\|\,\mathbf{u}\,\|^2}\right)\left(u_j\varphi_j\frac{\partial\varphi_k}{\partial x} + v_j\varphi_j\frac{\partial\varphi_k}{\partial y}\right)\mathrm{d}\omega\right)v_k \quad i = 1,\ldots,N, \tag{21}$$

$$\mathbf{d}(\mathbf{u})_{ik} = \sum_j\left(\int_\omega\left(\varphi_i + \frac{\tilde{k}\mathbf{u}\cdot\nabla\varphi_i}{\|\,\mathbf{u}\,\|^2}\right)\left(u_j\varphi_j\frac{\partial\varphi_k}{\partial x} + v_j\varphi_j\frac{\partial\varphi_k}{\partial y}\right)\mathrm{d}\omega\right) \quad i,k = 1,\ldots,N, \tag{22}$$

$$b_{u_i} = \int_{\partial\omega_A}\varphi_i\left[-pn_1 + \sum_j \mu(n_1u_j + n_2v_j)\frac{\partial\varphi_j}{\partial x}\right]\mathrm{d}s \tag{23}$$

$$b_{v_i} = \int_{\partial\omega_A}\varphi_i\left[-pn_2 + \sum_j \mu(n_1u_j + n_2v_j)\frac{\partial\varphi_j}{\partial y}\right]\mathrm{d}s + \mathrm{T_a}\sum_k\left[\int_\omega \varphi_i\varphi_k\,\mathrm{d}\omega\right]w_k^2 \tag{24}$$

$$b_{\phi_i} = \sum_j\sum_k\left[\int_\omega \mu E_c\varphi_i\left(\frac{\partial\varphi_j}{\partial x}\frac{\partial\varphi_k}{\partial x} + \frac{\partial\varphi_j}{\partial y}\frac{\partial\varphi_k}{\partial y}\right)\mathrm{d}\omega\right]w_jw_k, \; i = 1,\ldots,N \tag{25}$$

where $\tilde{k}$ is the coefficient of added diffusion (Brooks and Hughes 1982) and $\|\,\mathbf{u}\,\|^2 = \mathbf{u}\cdot\mathbf{u}$ is the modulus square of the velocity field. The index i in the line integrals of Equations 23 and 24 refers only to those nodes falling on the boundary $\partial\omega_A$.

Time-stepping algorithm

A simple reordering of the rows and columns of the element matrices, performed during the assembly procedure of the finite element method, minimizes the half-bandwidth of the stiffness matrix with the resulting saving in storage and computing time. Therefore, and for computational purposes only, the vector of unknown nodal velocities is first reordered as $\mathbf{u} = (u_1, v_1, u_2, v_2, u_N, v_N)$. On the other hand, and owing to the typical badly conditioned system of ordinary differential equations generated by the penalty method, a direct elimination method is used for Equations 13–14 (Carey and Oden 1986; Codina 1993). Moreover, the disparate size of the geometry under consideration may introduce difficulties analogous to those encountered in stiff systems. Unconditionally stable implicit methods in combination with Newton's linearization algorithm are good candidates for nonlinear problems that exhibit stiff behavior (Byrne and Hindmarsch 1987). Accordingly, Equations 13 and 14 are integrated forward in time with the backward-Euler scheme using a fixed time step Δt.

For every time level $t_n = n\Delta t$, the current value of the temperature $\underline{\boldsymbol{\Phi}}^n$ is used to compute the viscosity μ^n, the Prandtl number P_r^n, and the Eckert number E_c^n. Then, the velocity is computed by solving, for each νth iteration, the linear system

$$\mathbf{u}^{\nu+1} = \mathbf{u}^\nu + \Delta\mathbf{u}^\nu = \mathbf{u}^\nu - J(\mathbf{u}^\nu)^{-1}\underline{\mathbf{f}}(\mathbf{u}^\nu) \tag{26}$$

using a direct solver based on Gaussian elimination for unsymmetric banded matrices (Dongarra et al. 1979). Here, $J_{im} = \partial f_i/\partial u_m$ is the Jacobian matrix of the nonlinear vector

$$\underline{\mathbf{f}}(\mathbf{u}^{n+1}) = [M_o + \Delta tB(\mu^n)]\mathbf{u}^{n+1} + \Delta t\underline{\mathbf{c}}(\mathbf{u}^{n+1}) - [M_o\mathbf{u}^n + \Delta t\underline{\mathbf{b}}_{\underline{\mathbf{u}}}^n] \tag{27}$$

A convergence tolerance of less than 1% of the relative change $\|\,\Delta\mathbf{u}^\nu\,\|/\|\,\mathbf{u}^\nu\,\|$ is imposed to terminate each full Newton iteration, where $\|\,\mathbf{u}\,\| = \sum u_j, j = 1,\ldots,2N$. The dynamic pressure, approximated with piecewise constant elements, is computed over each element using the weak form of the penalty function approximation. The values of the velocity field $(\mathbf{u}^n, \underline{\mathbf{w}}^n)$ and the pressure $\underline{\mathbf{p}}^n$ are used to form the load vector $\underline{\mathbf{b}}_{\underline{\mathbf{u}}}{}^n$, which contains the FBC and the centrifugal acceleration term. Next, $\underline{\mathbf{w}}$ is updated via

$$\{M + \Delta t[D(\mathbf{u}^{n+1}) + A(\mu^n)]\}\underline{\mathbf{w}}^{n+1} = M\underline{\mathbf{w}}^n + \Delta t\mathbf{b}_{\underline{\mathbf{w}}}{}^n \tag{28}$$

and finally, the temperature is advanced by solving the following:

$$\left\{M + \Delta t\left[D(\mathbf{u}^{n+1}) + A\left(\frac{1}{P_r}\right)\right]\right\}\underline{\boldsymbol{\Phi}}^{n+1} = M\underline{\boldsymbol{\Phi}}^n + \Delta t b_{\underline{\boldsymbol{\Phi}}}^n(\underline{\mathbf{w}}^{n+1}) \tag{29}$$

The scheme is repeated until steady state is achieved. In the above equations, M_o is the lumped mass matrix of the block $2N \times 2N$ matrix defined in Equation (13); B is the $2N \times 2N$ matrix also defined in Equation 13; and $\underline{\mathbf{b}}_{\underline{\mathbf{u}}} = (\underline{\mathbf{b}}_{\mathbf{u}}, \underline{\mathbf{b}}_{\mathbf{v}})^T$.

Numerical experiments and discussion

An important parameter for seal designers is the temperature developed in the contact area. Experiments have shown that beyond a certain temperature that depends upon the thermophysical properties of the elastomer, a considerable wear takes place and with it, a decrease in seal service life (Stakenborg 1988). For temperatures ranging from 20°C to 80°C, the specific heat of a standard lubricating oil has a variation of approximately 13%; whereas the thermal conductivity has a variation of only 5%. These changes are small compared with a viscosity variation of more than 90% over the same temperature range. Consequently, while the P_r and the E_c numbers are held constant during the computations, an exponential decrease in viscosity with increasing temperature is assumed. On the other hand, the convective heat transfer coefficient is a rather complicated function of many variables, and not enough experimental information is available to determine its dependence. The asymptotic value $N_u = 5.385$ (Kays and Crawford 1987) could be used within the gap where the conditions of insulation and zero curvature are consistent with the boundary conditions and the small-gap limit proposed in this paper. However, the condition of a fully developed temperature profile is not necessarily achieved and, even more important, the asymptotic value 5.385 will change with the system geometry outside the contact region. In numbers, the rate of the convective heat transfer between the solid shaft and the fluid is characterized by the ratio $N_u/P_r = hd/\rho c v_o$, which for $h \sim 450$ W/m^{2}K and $\rho \sim 900$ kg/m^3, is on the order of 10^{-3}. A characteristic value $N_u = 1$ seems, therefore, plausible with the range of Prandtl number explored here. A bulk temperature of the oil in the sealed region of 40°C is assumed, and is set equal to the reference temperature T_o. The other parameter values used in the simulations are $T_\infty = 20$°C, $v_o = 6.73 \times 10^{-5}$ m^2/s; $c = 1800$ J/kg.K; $k = 0.145$ W/m.K, $h_o = 10$ μm; $b = 200$ μm; and $R = 0.035$ m. Note that the Taylor number and the Eckert number, both being a function of the angular velocity, are not independent. The ratio T_a/E_c is constant and equal to $cd^3(T_o - T_\infty)/v_o^2 R$.

The flow through the gap is analyzed for a variety of conditions with constant and variable viscosity. The geometry and, in particular, the extremely small size of the gap impose a severe constraint in the numerical simulation. Preliminary computations showed the necessity of using mesh grading as the contact region is approached from both sides. Transition elements are also employed to avoid extremely small elements in the contact area (Vionnet and Heinrich 1993a). All results are validated using meshes of different sizes to test the influence of the OBC on the numerical solutions. The final mesh contains 2,035 nodes and 1,864 bilinear quadrilateral elements. The pressure is adjusted at every step in such a way that is always zero at the first element (located at $x = -11$, $y = 0$), and the line integrals in Equations 24–25 are evaluated, as the OBC requires, with values computed on the elements located along the outflow boundaries.

Results of the axial velocity component, the circumferential velocity component, and the temperature obtained with the FBC for both constant and variable viscosity, are shown in Figure 3. The typical parameter values considered for the numerical experiments are listed in Table 1. The temperature distribution within the microgap is shown for different values of the Brinkman number $B_r = P_r E_c$. A local solution based on the pressure gradients obtained numerically is plotted in Figure 3a to show that the flow within the gap is, indeed, fully developed when the viscosity is held constant (Table 1). For the Prandtl numbers considered here (Table 2), no major variations are observed in the flow within the gap when the viscosity is allowed to vary with temperature (Figures 3d–f). Hence, the comparison between the constant viscosity case and the variable viscosity case is now restricted to the common values $T_a = 3$, $E_c = 0.0017$, and $P_r = 1000$. It can be seen from Figure 4 that the constant properties model (a) predicts a temperature peak much higher than the variable properties model (b). The local maximum is better appreciated in Figure 5. The overall effect of the temperature is to increase the effect of the inertial forces by lessening the viscous resistance on the oil side of the contact area. As a result, a higher sealing pressure on the air side is induced (Figure 6). This shows rather conclusively that sealing is, indeed, a dynamic mechanism. This can be appreciated in Figure 7 where only the constant viscosity case is shown (the projection of the variable viscosity solution differs from that shown in Figure 7 only by a stretching factor). The velocity field and stream function contours on the air side, obtained when the FBC is employed, are shown in Figure 8. Figure 9 shows analogous results for the same parameter values when the NBC is used instead. The effect is so dramatic as to reverse the direction of the flow within the gap. Although the NBC solution suggests leakage, the FBC solution indicates that sealing is achieved by pumping oil from the air side, where the azimuthal flow is stable, to the oil side where instabilities set in (Figure 10). In all cases a typical temperature peak of approximately 200°C is obtained for the constant properties model, and of 80°C for the variable properties model. It is clear that viscous dissipation effects are overestimated when the viscosity is held constant during the computation. Stakenborg (1988) estimated an approximate upper bound of 90°C for the temperature under normal operation.

Regardless of interfacial effects on the air side, the boundary condition applied here mimics the conditions encountered in experiments where the air side is continuously fed with fluid to determine the pumping rate. The treatment of the open boundaries as described briefly in this work has proved reliable in a variety of situations. It is known that the use of the NBC in presence of variable body forces leads to erroneous results (Vionnet and Heinrich 1993b). On the contrary, the application of the FBC achieves a precise balance of forces by keeping the pressure on the line integral defined along the boundary of the artificially truncated domain. To some extent, this OBC is insensitive to the location of the open boundaries (Vionnet 1993). Moreover, it is not hard to show that, for 1-D convection–diffusion problems, the FBC is equivalent to a radiating boundary able to filter unwelcome reflections toward the interior of the computational domain (Sani and Gresho 1994, Heinrich and Vionnet 1995).

Finally, whereas the present small-gap limit yields an axisymmetric flow field, the shape of the gap may vary along the azimuthal angle θ in response to the elastic nature of the seal. Therefore, it is relevant to impose upper bounds on some of the parameters for the limit $\delta \to 0$ to be a valid approximation. This can be accomplished, as is common practice in fluid mechanics, with the help of the solution itself. In the gap region, the numerical solution represents a plane Couette flow (Figure 3b and 3e), which, after being rescaled with h_o instead of d, can be expressed as $u_\theta = U[1 - (r - R)/h_o]$ where $U = \Omega R$ is the sliding velocity of the rotary shaft. It follows that a typical order of magnitude of the neglected inertia term $u_\theta \partial u_\theta/\partial s$ is $\alpha U^2/h_o$. Here, α characterizes the angle between the two bodies (i.e., $\alpha = \partial h_o/\partial s$) and $s = R\theta$ is the arc length (Figure 1). On the other hand, the viscous force retained in the equations of motion, which for the constant properties model is $v_o \nabla^2 u_\theta$, can be well estimated by $v_o U/h_o^2$. The small-gap limit is, therefore, a consistent approximation to the equations of motion in the event the ratio $\alpha R_e \ll 1$, where R_e is the Reynolds number based on h_o. In the present formulation, both α and the product αR_e, sometimes termed the modified Reynolds number, are required to be small. These requirements are the well-known limitations imposed on the Reynolds lubrication theory. Furthermore, the Taylor number written in terms of h_o, $T_a = \delta R_e^2$, shows that centrifugal effects are indeed negligible within the gap. In contrast, the numerical results show that curvature and centrifugal effects are the leading mechanisms outside the contact region, where the lubrication approximation ceases to be valid.

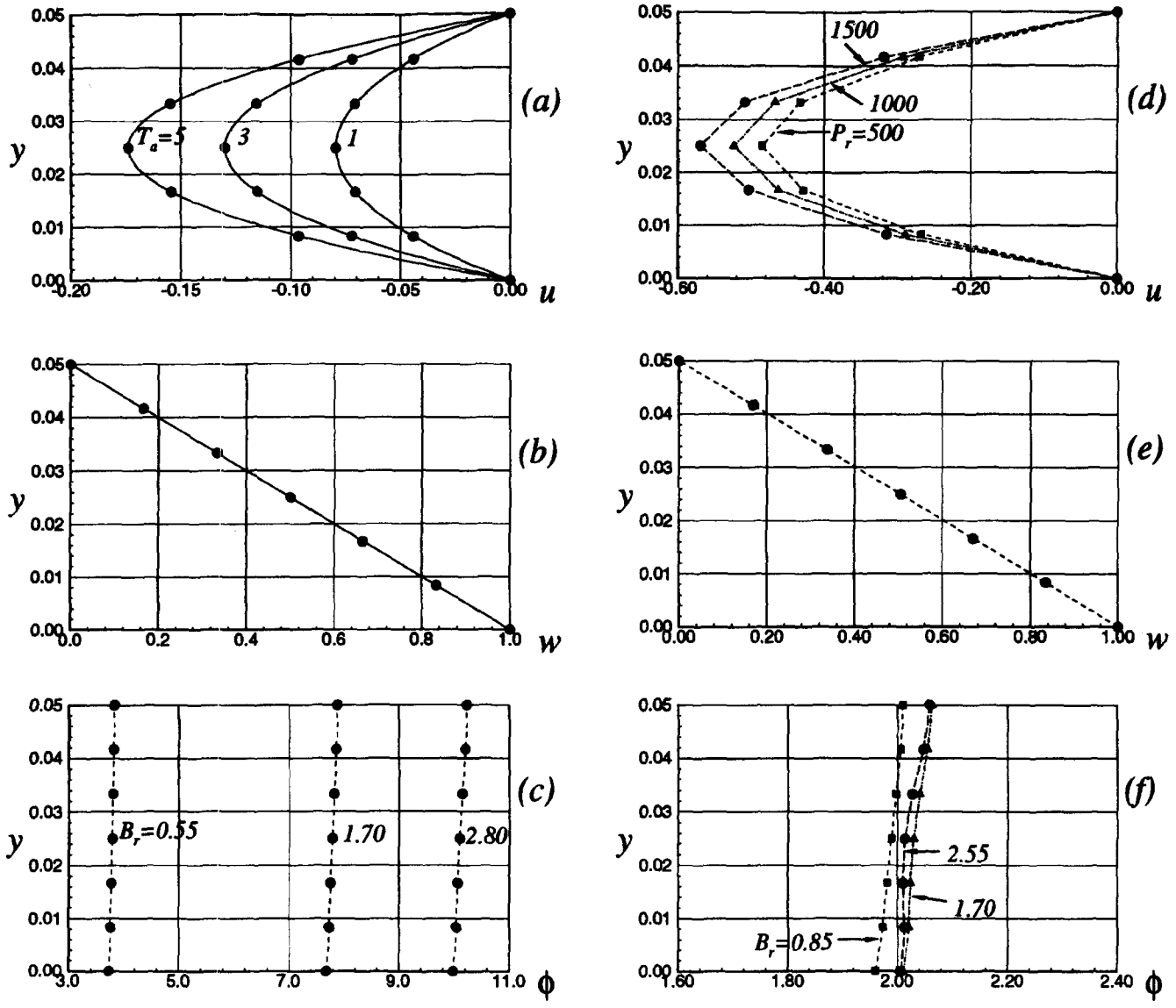

Figure 3 Solution at $x = 0.5$ for the constant viscosity case (a–c); solution at $x = 0.5$ for the variable viscosity case (d–f)

Table 1 Constant viscosity $P_r = 1000$

T_c	1	3	5
E_c	5.5×10^{-4}	1.7×10^{-3}	2.8×10^{-3}
B_r	0.55	1.70	2.80
$\Delta p/\Delta x$	254.2	415.5	556.0

Table 2 Variable viscosity, $T_a = 3$, $E_c = 1.7 \times 10^{-3}$

P_r	500	1000	1500
B_r	0.85	1.70	2.55

Closure

Besides illustrating its simplicity, the appropriateness of the small-gap limit in capturing the underlying forces that drive the flow of lubricant through the gap of shaft seals has been established. In physical terms, the parameters needed to describe the system have been reduced to the angular velocity and some temperature difference, or in dimensionless term, to the Taylor number and the Prandtl number.

It was shown that for a small ratio of gap size to shaft radius, the motion of the fluid underneath a radial lip seal gives rise to a superposition of a secondary flow in the axial plane an a pure shearing motion in the azimuthal direction. Furthermore, the small-gap limit says that the flow through the gap is totally determined by an axial pressure gradient induced by Taylor vortices on the oil side, and by a quasihydrostatic pressure distribution on the air side. This constitutes a rather simple but remarkable observation, considering that the main body of the literature has emphasized only the role played by seal asperities on the sealing mechanism.

Both the free and the stress-free boundary conditions show that centrifugal instabilities are an important driving force in the sealing mechanisms of shaft seals, even when their predictions are contradictory. In particular, special care must be taken with the stress-free boundary condition because of its inherent lack of reaction to body forces at open boundaries. In contrast, the free boundary condition as used in this work indicates that sealing is achieved by pumping oil from the air side, where the almost plane Couette flow is stable, to the oil side, where Taylor instabilities set

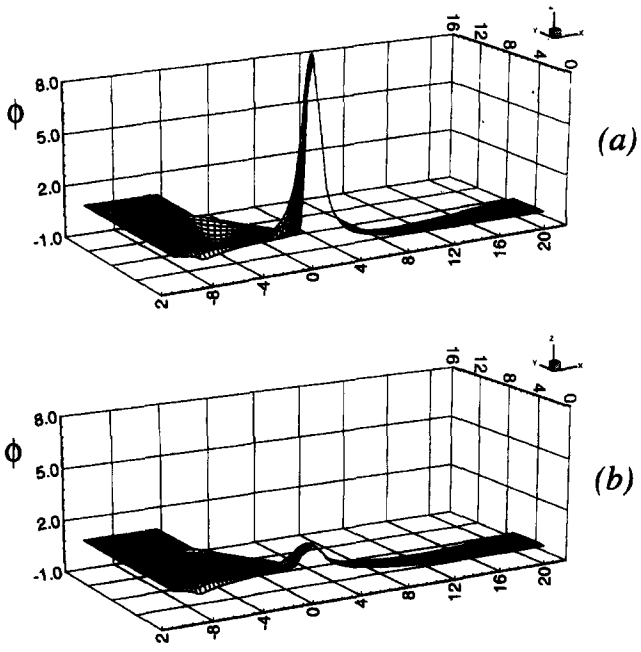

Figure 4 Temperature distribution, (a) constant viscosity, (b) variable viscosity

in. The strength of the recirculating cell observed on the air side is not enough to reverse the flow direction when thermal effects are taken into account. However, a further increase in the Prandtl number may, indeed, change the balance of forces, and leakage may occur. This and other effects, such as cavitation and interfacial forces, should be included in future works.

Appendix

The Navier–Stokes equations for a nonisothermal, incompressible Newtonian fluid of uniform density, and written in cylindrical

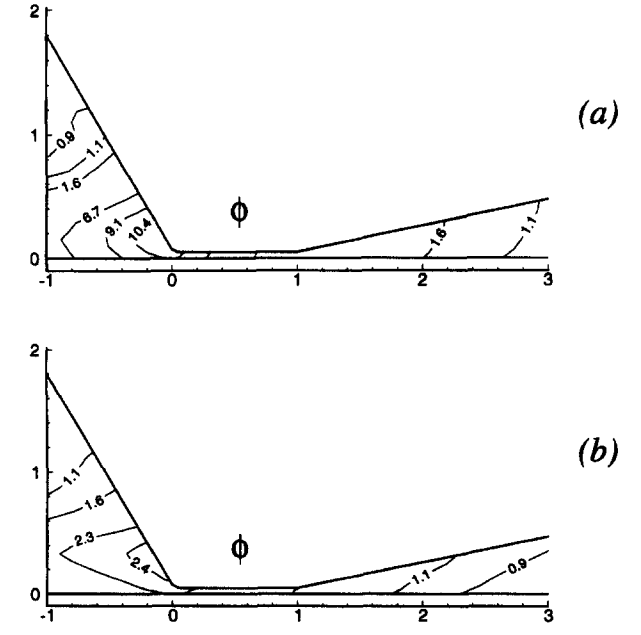

Figure 5 Temperature contours in the gap region, (a) constant viscosity, (b) variable viscosity

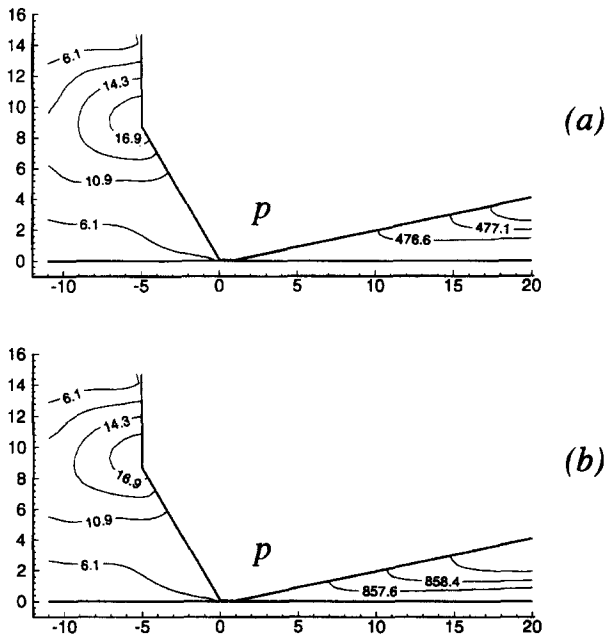

Figure 6 Pressure contours, (a) constant viscosity, (b) variable viscosity

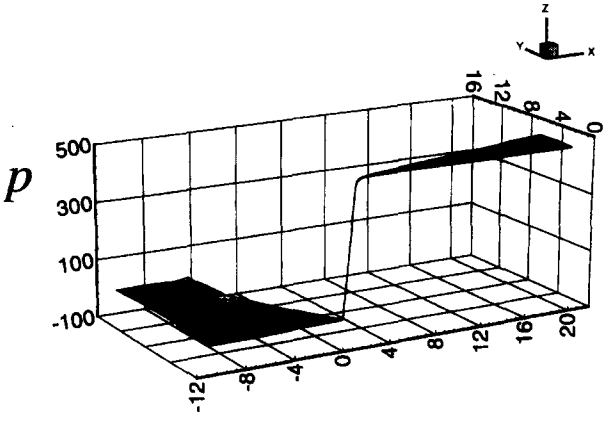

Figure 7 Pressure distribution for the constant viscosity case

coordinates with the line $r=0$ coincident with the shaft axis, are (Bird et al. 1960)

$$\frac{\partial u_z}{\partial z}+\frac{1}{r}\frac{\partial (ru_r)}{\partial r}+\frac{1}{r}\frac{\partial u_\theta}{\partial \theta}=0$$

$$\rho\left(\frac{\partial u_z}{\partial t}+\mathbf{u}.\mathrm{grad}(u_z)\right)=-\frac{\partial p^*}{\partial z}+\frac{1}{r}\frac{\partial (r\tau_{rz})}{\partial r}+\frac{1}{r}\frac{\partial \tau_{\theta z}}{\partial \theta}+\frac{\partial \tau_{zz}}{\partial z}$$

$$\rho\left(\frac{\partial u_r}{\partial t}+\mathbf{u}.\mathrm{grad}(u_r)-\frac{u_\theta^2}{r}\right)=-\frac{\partial p^*}{\partial r}+\frac{1}{r}\frac{\partial (r\tau_{rr})}{\partial r}+\frac{1}{r}\frac{\partial \tau_{r\theta}}{\partial \theta}-\frac{\tau_{\theta\theta}}{r}+\frac{\partial \tau_{rz}}{\partial z}$$

$$\rho\left(\frac{\partial u_\theta}{\partial t}+\mathbf{u}.\mathrm{grad}(u_\theta)+\frac{u_r u_\theta}{r}\right)=-\frac{1}{r}\frac{\partial p^*}{\partial \theta}+\frac{1}{r^2}\frac{\partial (r^2\tau_{r\theta})}{\partial r}+\frac{1}{r}\frac{\partial \tau_{\theta\theta}}{\partial \theta}+\frac{\partial \tau_{\theta z}}{\partial z}$$

$$\rho c\left(\frac{\partial T}{\partial t}+\mathbf{u}.\mathrm{grad}(T)\right)=\frac{\partial}{\partial r}\left(k\frac{\partial T}{\partial r}\right)+\frac{k}{r}\frac{\partial T}{\partial r}+\frac{1}{r}\frac{\partial}{\partial \theta}\left(\frac{k}{r}\frac{\partial T}{\partial \theta}\right)+\frac{\partial}{\partial z}\left(k\frac{\partial T}{\partial z}\right)$$
$$+2\mu\left[\left(\frac{\partial u_r}{\partial r}\right)^2+\frac{1}{r^2}\left(\frac{\partial u_\theta}{\partial \theta}+u_r\right)^2+\left(\frac{\partial u_z}{\partial z}\right)^2\right]+\mu\left(\frac{\partial u_\theta}{\partial z}+\frac{1}{r}\frac{\partial u_z}{\partial \theta}\right)^2$$
$$+\mu\left\{\left(\frac{\partial u_z}{\partial r}+\frac{\partial u_r}{\partial z}\right)^2+\left[\frac{1}{r}\frac{\partial u_r}{\partial \theta}+r\frac{\partial}{\partial r}\left(\frac{u_\theta}{r}\right)\right]^2\right\}$$

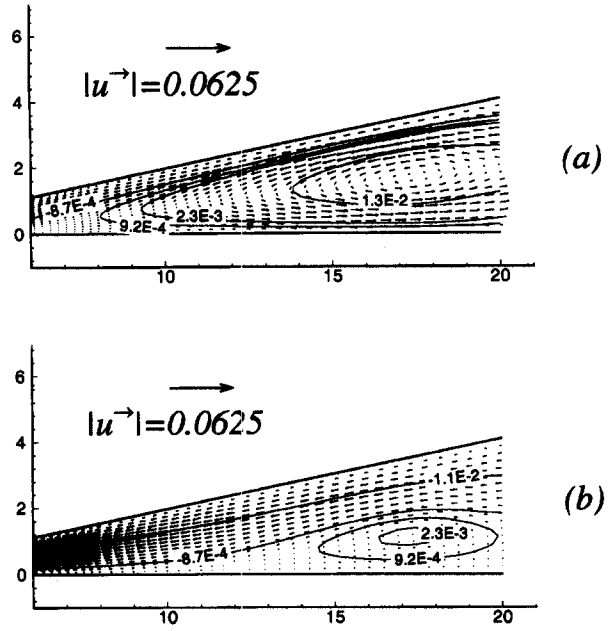

Figure 8 Velocity field and stream function contours on the air side when the FBC is used at the outflow boundaries, (a) constant viscosity, (b) variable viscosity

where $\mathbf{u} = (u_z, u_r, u_\theta)$ is the velocity vector in the z, r, θ directions, respectively, and $\text{grad} = (\partial_z, \partial_r, \frac{1}{r}\partial_\theta)$ is the gradient operator. The components of the viscous stress tensor are given by the following:

$$\tau_{rr} = 2\mu^* \frac{\partial u_r}{\partial r} \qquad \tau_{r\theta} = \tau_{\theta r} = \mu^* \left(r \frac{\partial}{\partial r}\left(\frac{u_\theta}{r}\right) + \frac{1}{r}\frac{\partial u_r}{\partial \theta} \right)$$

$$\tau_{\theta\theta} = 2\mu^* \left(\frac{1}{r}\frac{\partial u_\theta}{\partial \theta} + \frac{u_r}{r} \right) \qquad \tau_{\theta z} = \tau_{z\theta} = \mu^* \left(\frac{1}{r}\frac{\partial u_z}{\partial \theta} + \frac{\partial u_\theta}{\partial z} \right)$$

$$\tau_{zz} = 2\mu^* \frac{\partial u_z}{\partial z} \qquad \tau_{rz} = \tau_{zr} = \mu^* \left(\frac{\partial u_r}{\partial z} + \frac{\partial u_z}{\partial r} \right)$$

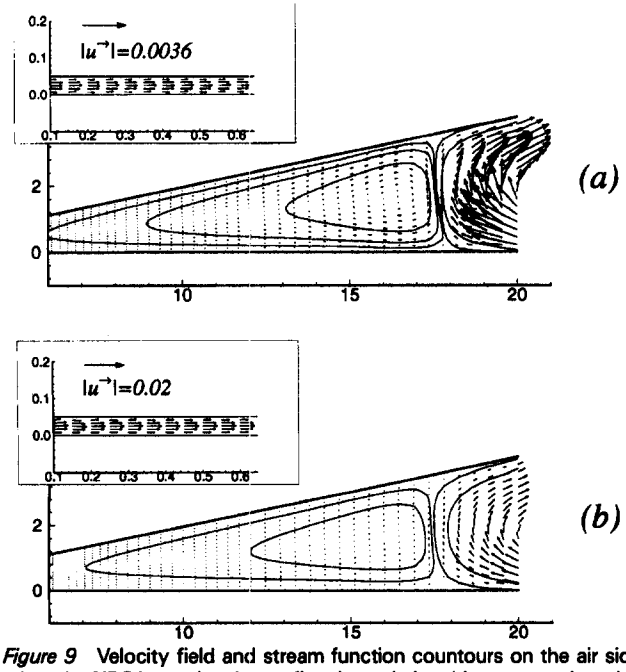

Figure 9 Velocity field and stream function countours on the air side when the NBC is used at the outflow boundaries, (a) constant viscosity, (b) variable viscosity

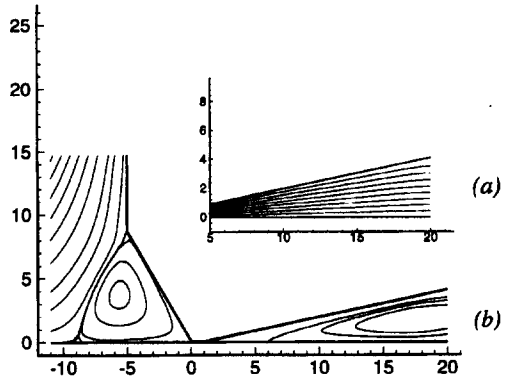

Figure 10 Constant viscosity solution obtained with the FBC, (a) contour lines of the azimuthal component of the velocity on the air-side, (b) stream function contours

In absence of a free surface, the gravitational body force is expressed as the gradient of a scalar quantity, and, therefore, it has been included in the pressure gradient term.

References

Bird, B. R., Stewart, W. E. and Lightfoot, E. N. 1960. *Transport Phenomena*. Wiley, New York

Brooks, A. N. and Hughes, T. J. R. 1982. Streamline upwind/Petrov Galerkin formulations for convection dominated flows with particular emphasis on the incompressible Navier–Stokes equations. *Comp. Methods Appl. Mech. Eng.*, **32**, 199–259

Byrne, G. and Hindmarsh, A. C. 1987. Stiff ODE solvers: A review of current and coming attractions. *J. Comp. Phys.*, **70**, 1–62

Carey, G. F. and Oden, J. T. 1986. *Finite Elements. Fluid Mechanics*, Vol. VI, Prentice-Hall, Englewood Cliffs, NJ

Chandrasekhar, S. 1961. *Hydrodynamic and Hydromagnetic Stability*. Dover, New York

Christie, I., Griffiths, D. F., Mitchell, A. R. and Sanz-Serna, J. M. 1981. Product approximation for non-linear problems in the finite element method. *IMA J. Num. Analysis*, **1**, 253–266

Codina, R. 1993. An iterative penalty method for the finite element solution of the stationary Navier–Stokes equations. *Comp. Methods Appl. Mech. Eng.*, **110**, 237–262

Dongarra, J. J., Bunch, J. R., Moler, C. B. and Stewart, G. W. 1979. *LINPACK User's Guide*, SIAM, Philadelphia

Gresho, P. M. and Sani, R. L. 1990. Introducing four benchmark solutions. *Int. J. Num. Methods Fluids*, **11**, 951–952

Hall, P. 1975. The stability of unsteady cylinder flows. *J. Fluid Mech.*, **67**, 29–63

Heinrich, J. C. and Vionnet, C. A. 1995. On boundary conditions for unbounded flows. *Comm. Appl. Num. Methods*, **11**, 179–185

Hughes, T. J. R., Liu, W. K. and Brooks, A. 1979. Finite element analysis of incompressible viscous flows by the penalty function formulation. *J. Compt. Phys.*, **30**, 1–60

Jagger, E. T. 1957. Rotary shaft seals: The sealing mechanism of synthetic rubber seals running at atmospheric pressure. *Proc. Inst. Mech. Eng.*, **171**, 597–616

Jagger, E. T. and Walker, P. S. 1966. Further studies of the lubrication of synthetic rubber shaft seals. *Proc. Inst. Mech. Eng.*, **181**, 101–204

Kawahara, Y., Abe, M. and Hirabayashi, H. 1980. An analysis of sealing characteristics of oil seals. *ASLE Trans.*, **23**, 93–102

Kawahara, Y. and Hirabayashi, H. 1977. A study of sealing phenomena on oil seals. *ASLE 77-LC-5B-2*, ASLE/ASME Lubrication Conference, Kansas City.

Kelly, D. W., Nakazawa, S., Zienkiewics, O. C. and Heinrich, J. C. 1980. A note on upwinding and anisotropic balancing dissipation in finite element approximations to convective diffusion problems. *Int. J. Num. Methods Eng.*, **15**, 1705–1711

Kays, W. M. and Crawford, M. E. 1987. *Convective Heat and Mass Transfer*. McGraw-Hill, New York, 101

Lebeck A. O. 1986a. Parallel sliding load support in the mixed friction regime. Part 1. The Experimental Data. *J. Tribology*, **109**

Lebeck A. O. 1986b. Parallel sliding load support in the mixed friction regime. Part 2. Evaluation of the Mechanism. *J. Tribology*, **109**

Oh, K. P. and Rohde, S. M. 1977. Numerical solution of the point contact problem using the finite element method. *Int. J. Num. Methods Eng.*, **11**, 1507–1518

Papanastasiou, T. C., Malamataris, N. and Ellwood, K. 1992. A new outflow boundary condition. *Int. J. Num. Methods Fluids*, **14**, 587–608

Prati, E. and Strozzi, A. 1984. A study of the elastohydrodynamic problem in rectangular elastomeric seals. *J. Tribology*, **106**, 505–512

Ruskell, L. E. C. 1980. A rapidly converging theoretical solution of the elastohydrodynamic problem for rectangular rubber seals. *J. Mech. Eng. Sci.*, **22**, 9–16

Salant, R. F. 1992. Numerical analysis of the flow field within lip seals containing micromodulations. *J. Tribology*, **114**, 485–492

Salant, R. F. and Flaherty, A. L. 1995. Elastohydrodynamic analysis of reverse pumping in rotary lip seals with microasperites. *J. Tribology*, **117**, 53–59

Sani, R. L. and Gresho, P. M. 1994. Résumé and remarks on the open boundary condition minisymposium. *Int. J. Num. Methods Fluids*, **18**, 983–1008

Serbetci, I. and Tichy, J. A. 1991. Inertial effects in thin film flow with a corrugated boundary. *J. App. Mech.*, **58**, 272–277

Stakenborg, M. J. L. 1988. On the sealing and lubrication mechanism of radial lip seals. Ph.D Dissertation, Eindhoven University of Technology, The Netherlands.

Taylor, C. and O'Callaghan, J. F. 1972. A numerical solution of the elastohydrodynamic lubrication problem using finite elements. *J. Mech. Eng. Sci.*, **14**, 229–237

Veronis, G. 1967. Analogous behavior of homogeneous, rotating fluids and stratified, non-rotating fluids. *Tellus*, **XIX**, 326–335

Verstappen, R. and van Groesen, E. 1989. On the consistent formulation and approximation of EHL theory. *J. Tribology*, **111**, 109–113

Vionnet, C. A. 1993. Analysis of lubricant flows within the microgap of rotary lip seals. Ph.D. Dissertation. The University of Arizona. Tucson, Arizona

Vionnet, C. A. and Heinrich, J. C. 1993a. An application of small-gap equations in sealing devices. *NASA Conference Publication 10122*, 499–512

Vionnet, C. A. and Heinrich, J. C. 1993b. Open boundary conditions for viscous flows with variable body forces. In *Advances in Finite Element Analysis in Fluid Mechanics*, M. Dhaubhadel et al. (eds.), ASME, New York, 39–45